Reentry CubeSat Heatshield Monitoring System Using Fiber Bragg Gratings

Vanhamel , Jurgen

DOI
10.1109/OJIM.2025.3569358

Publication date
2025

Document Version
Final published version

Published in
IEEE Open Journal of Instrumentation and Measurement

IEEE Open Journal of Instrumentation and Measurement

Received 11 April 2025; revised 23 April 2025; accepted 30 April 2025. Date of publication 15 May 2025; date of current version 27 May 2025.
The review of this paper was arranged by Associate Editor Eric Fujiwara.

Digital Object Identifier 10.1109/OJIM.2025.3569358

Reentry CubeSat Heatshield Monitoring System Using Fiber Bragg Gratings

JURGEN VANHAMEL[1,2] (Senior Member, IEEE), KIN CHIO CHAO[3], AND YIFENG CHEN[3]

[1]Faculty of Aerospace Engineering, TU Delft, 2629 HS Delft, The Netherlands
[2]Advanced Integrated Sensing Lab, Department of Electrical Engineering (ESAT), KU Leuven, 3000 Leuven, Belgium
[3]Faculty of Engineering Technology, Campus Group T, KU Leuven, 3000 Leuven, Belgium

CORRESPONDING AUTHOR: J. VANHAMEL (e-mail: j.a.m.vanhamel@tudelft.nl)

This work was supported in part by the Faculty of Aerospace Engineering, TU Delft, The Netherlands, and in part by the Advanced Integrated Sensing Lab, Department of Electrical Engineering, KU Leuven, Belgium.

ABSTRACT In space applications, CubeSats are used for all kinds of commercial and research purposes. These small satellites are launched in such large numbers that from a pollution point of view it makes sense to return them intact to Earth. To establish this, a dedicated reentry is needed. During this reentry process, the CubeSat has to make use of a heatshield which deforms due to multiple forces acting upon the structure. In order to monitor this heatshield, this study aims at investigating, designing, simulating, and testing the integration and readout of fiber Bragg gratings (FBGs) into a mock-up heatshield, in order to monitor its shape. Therefore, a mock-up of a CubeSat and its accompanying heatshield is constructed to simulate the realistic use of FBGs. Based on the external dimensions of the heatshield, the study gives a practical installation pattern for the FBGs. A 3-D simulation model of the heatshield and accompanying CubeSat is built. To achieve deformation in this 3-D model, the study proposes an algorithm based on single-point data. Using existing OROCOS/ROS middleware, the study establishes a comprehensive system for setting up and reading out FBGs in order to gather information on the heatshield's status. Finally, after testing the mock-up heatshield set, the system can reflect the deformation of the heatshield in real-time in the 3-D model. Additionally, the system can save the entire deformation process of the heatshield as a series of model files, which can be used for sophisticated static analysis.

INDEX TERMS CubeSat, fiber Bragg grating (FBG), heatshield, monitoring, reentry.

I. INTRODUCTION

A CUBESAT is an affordable platform usable for commercial, educational, and research purposes [1]. These low-cost, versatile, and efficient platforms are used for Earth observation [2], communication [3], deep space research [4], as well as for space weather monitoring [5]. Another feature is its small size of 10 × 10 × 10 cm for one unit (1U), making these platforms suitable for small sample return using a reentry system [6]. For example, biological experiments carried out aboard the International Space Station (ISS) could be returned to Earth, using a reentry CubeSat. This allows a flexible and low-cost transportation system for sample return [7]. A 3U reentry CubeSat would consist of a deployable heatshield housed in the top unit of the CubeSat (1U), together with a payload bay for the samples (1U) and the onboard systems (1U) [7] (Fig. 1). The heatshield consists of an inflatable cone with the inflatable ring located at the bottom of the cone and a nose cone at the top of the CubeSat (Fig. 1). When the heatshield is used, the ring at the bottom of the cone is gradually filled with gas and eventually fully expanded.

The structural integrity of the CubeSat's heatshield is critical during the reentry process. Extreme space conditions can seriously affect the status of the heatshield. In order to have a better view on this status, a monitoring system can be integrated inside the heatshield, enabling the measurement of parameters, such as temperature, stress, and strain. In order to do so, conventional thermal and pressure sensors can be used [8]. Accelerometers can be embedded in the heatshield for measuring structural stresses and deformation during reentry [9]. Additionally, camera systems can be used for health monitoring purposes [10], although these systems can only be

installed on larger spacecrafts. Due to extreme temperature differences in space and the various types of radiation, the lifetime of sensors can be significantly reduced. Furthermore, violent vibrations during the launch of the satellite may damage the sensor systems and render them ineffective.

Fiber Bragg gratings (FBGs) can withstand this harsh environment of space and can be used to build a shape monitoring system for heatshields during reentry [7]. FBGs are passive sensors, not requiring an electrical supply to acquire data. Moreover, they are insensitive to electromagnetic interference and have a high signal-to-noise ratio and measurement accuracy [11]. FBGs are lightweight, immune to electromagnetic interference, and flexible in installation, making them ideal for space missions with stringent weight and space requirements [12]. FBGs are already widely used in structural health inspection systems for other scenarios, such as bridges and pipelines [13], [14]. FBGs are not yet widespread in mobile structures, because the need of an associated interrogator, which is not always easy to integrate into the system [15]. The use of FBGs in space and space-related applications is slowly increasing [12], [16].

This work explores a new concept in which FBGs are used to monitor the health of a heatshield during the reentry process, specifically focusing on the applied forces. This article first describes the working principle of FBGs, consequently their respective characteristics and the selection of space-related FBGs. The study then focuses on a 3-D simulation, followed by the building, readout, and real-time linking to the 3-D model of a monitoring system, using FBGs integrated into a mock-up heatshield. Finally, this article concludes and suggests future directions for further improvement.

II. FIBER BRAGG GRATINGS

A. WORKING PRINCIPLE

An FBG is an optical filter that selectively reflects light at a specific wavelength, acting as a band-rejection filter. The wavelength of reflected light is determined by the spacing of the periodic refractive index variations, or grating, within the fiber core. This grating allows all wavelengths that do not match its resonance condition to pass through while reflecting those wavelengths that meet the Bragg condition established by the core's index modulation [7].

FBGs operate on the principle of Bragg diffraction, in which light of a specific wavelength is reflected by the periodic refractive index changes within the fiber itself [7]. This selective reflection is described by the Bragg condition, which can be stated as

$$\lambda_B = 2n_{eff}\Lambda \tag{1}$$

in which λ_B is the Bragg wavelength, n_{eff} is the effective refractive index of the fiber core, and Λ is the periodic spacing between the refractive index variations [7]. When the grating is subjected to an external force, resulting in an axial strain, a change occurs in the Bragg wavelength $\Delta\lambda_B$. This is reflected in (2) [10]

$$\Delta\lambda_B = 2n_{eff}\Lambda(1-\rho_e)\varepsilon \tag{2}$$

in which ρ_e is the effective strain-optic coefficient of the fiber core material, while ε is the longitudinal strain.

Based on the definition of strain ε, the latter can be rewritten as [17]

$$\varepsilon = \frac{\Delta\lambda_B}{\lambda_B(1-\rho_e)} = \frac{\Delta l}{l} \tag{3}$$

in which l and Δl are the original length and the change in length, respectively [17]. Using the relationship between strain ε and stress (σ), the force (F) exerted on the ends of a section of fiber can be calculated by

$$F = \varepsilon \,.\, E \,.\, A = \frac{\Delta\lambda_B}{\lambda_B(1-\rho_e)}.\, E \,.\, A \tag{4}$$

in which E is Young's modulus and A the cross section of the fiber. Hence, the force can be calculated based on FBGs.

Additionally, the effective refractive index n_{eff} and the periodic spacing Λ are temperature dependent, allowing the measurement of temperature variations with FBGs. The refractive index of the core is affected by both the thermo-optical coefficient and the coefficient of thermal expansion of the fibers. Hence, the temperature change can be detected. In the presence of both temperature and strain, the varying wavelength $\Delta\lambda_B$ can be obtained from the resonant wavelength λ_B, the strain ε, and the temperature variation ΔT [17]

$$\frac{\Delta\lambda_B}{\lambda_B} = (1-\rho_e)\varepsilon + \left(a_s + a_f\right)\Delta T \tag{5}$$

in which a_s is the coefficient of thermal expansion, and a_f is the thermo-optic coefficient.

B. FBG SETUP FOR SPACE APPLICATIONS

Due to the excellent characteristics, FBGs are used in aerospace projects up to a certain limit [18], [19]. The advantages of using FBGs in space include: 1) high immunity to electromagnetic interference, which effectively isolates the effects of cosmic radiation on measurement results; 2) lightweight; 3) flexible mounting positions and potential for embedding in recessed structures; 4) multiparameter sensing; and 5) multiple sensors can be effectively multiplexed, significantly reducing the overall power consumption of the sensing system [20].

In addition, unlike traditional sensors, FBGs are passive, meaning they do not require power to drive them. The only element that needs to be powered is the interrogator connected to the FBGs [7], [10], [21]. This interrogator is responsible for generating the light spectrum propagating inside the fiber and decoding the reflected wavelengths.

Fiber Coating Material Selection: The unique environment of space forces a dedicated choice in fiber material. A tradeoff is needed between the fiber harness protection level

and the weight of the sensor. Two main types of coating materials are used in fiber-optic sensors: 1) metal and 2) polymer [14], [22]. Polymers are the better choice for aerospace equipment where lightweight is desired. Hence, polyimide tubed fiber is used for its outstanding properties. Polyimide has high- and low-temperature resistance, excellent mechanical properties, is radiation resistant, is flexible, and has excellent dielectric properties [23].

Grating Selection: Six main types of FBG gratings exist: 1) uniform positive-only index change; 2) Gaussian apodized; 3) raised-cosine apodized; 4) chirped; 5) discrete phase shift; and 6) superstructure, each with their pros and cons [24]. Different grating structures are associated with different refractive index offsets and refractive index distribution properties. In general, there is a tradeoff between data accuracy and data volume in the choice of the grating. Denser grating numbers and more complex grating structures mean more accurate measurement data, larger data transfers, and more complicated data processing [14], [17]. Given the limited computing power that a CubeSat has and the real-time nature of the structural monitoring required, a relatively small amount of data should be used to build an accurate model that reflects the deformation of the heatshield surface. Consequently, the measurement points of the FBGs need to be spread over the heatshield's surface as much as possible to obtain the overall model parameters [6]. Therefore, superstructure FBGs (SFBGs) are the preferred choice because they generate less measurement data compared to other FBGs and do not require complex data handling processes [25]. Additionally, due to the unique structure of SFBGs, it is also possible to carry out multiparameter measurements, such as simultaneously measuring the surface structure strain and temperature [26].

Core Selection: It is crucial to consider the effects of high temperatures. Specifically, it is important to note that silica index gratings can become unstable at temperatures exceeding 400 °C and may completely disappear at 900 °C. For this reason, sapphire optical fibers are a more stable choice for high-temperature applications [27]. However, the applied heatshield will absorb most of the generated heat, hence, the estimate is that FBGs having temperature ranges between 200 °C and 300 °C are sufficient. Consequently, silica fibers are sufficient as a core.

Interrogator: The interrogator consists of two main components: 1) the transmitter and 2) the receiver. The transmitter generates optical signals traveling through the optical fiber, modulating the signals based on the measured parameter. This signal generation is done by using LEDs or laser diodes. The receiver detects the modulated signals using PIN diodes and converts these signals into electrical signals for further processing and analysis [28].

C. FBG HEATSHIELD INTEGRATION

As shown in Fig. 1, the conical structure of the heatshield is well supported at the bottom and top by the inflatable ring and the nose cone. Therefore, large deformations on the heatshield are most likely to occur in between these two

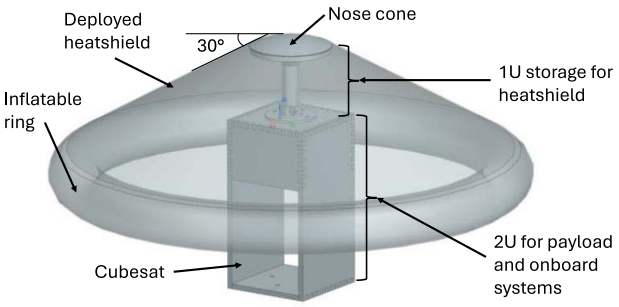

FIGURE 1. CubeSat with deployed heatshield.

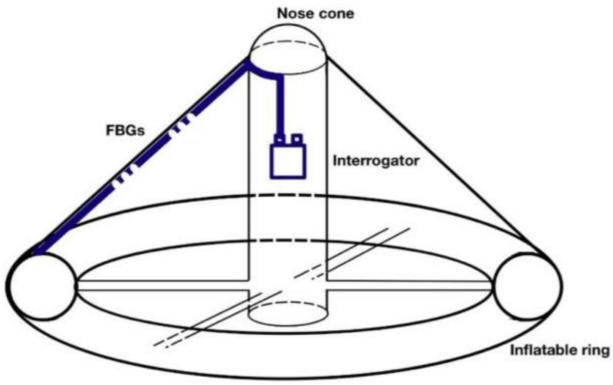

FIGURE 2. FBG integration into the heatshield.

parts. For this reason, the best mounting position for the FBGs is along the longitudinal side of the cone, which also allows the sensor to be well fixed at both ends using the nose cone and the inflatable ring (Fig. 2). In addition, as the transmitter–receiver end of the sensor is sensitive, this side should be placed under the nose cone to obtain maximum protection.

When using FBGs for surface measurements, it is important to consider the integration of the sensor into the structure. Specifically, the adhesive between the FBG and the surface of the structure to be measured must be able to transfer the strain from the structure to the sensor in an accurate way. Several bonding techniques exist, such as the use of specific glues [29] and epoxy resins with special heat treatments [30].

Another option is to embed the FBG in the composite structure. Embedded sensors can better reflect the strain changes in the structure. However, due to the strong inhomogeneities within the composite material, FBG misalignment with the local layers within the structure can cause distortion of the reflection spectrum [20]. Furthermore, embedded sensors have the disadvantage that the repair of the sensor is hard, meaning that once the sensor is damaged, the entire structure may have to be replaced.

III. SIMULATION OF HEATSHIELD PARAMETERS

The heatshield and the FBG setup, using traditional FBGs, is simulated using Python in the freely available, open-source 3-D computer graphics software tool called Blender [31].

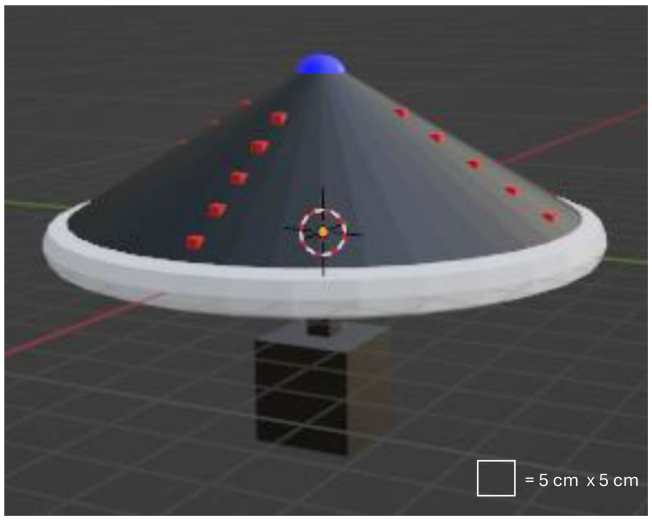

FIGURE 3. Heatshield model and FBG locations (red cubes).

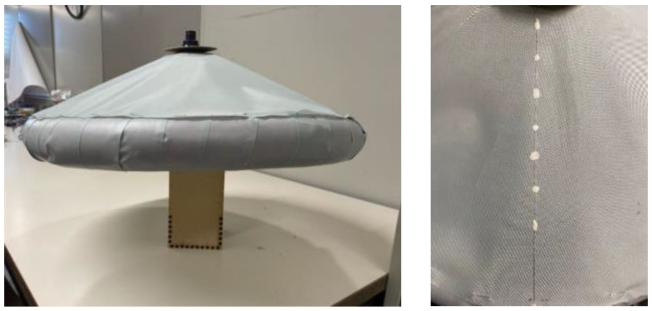

(a) (b)

FIGURE 4. (a) Heatshield and CubeSat mock-up. (b) Multicore fiber integration onto the heatshield.

By using a combination of facets, the heatshield shape is modeled in 3-D. Additionally, the inflatable ring is created using Blender's built-in ring model, while the nose cone is created by using Blender's sphere model. Finally, the construction of the CubeSat itself is also integrated into the model (Fig. 3).

To simulate the concept, the FBGs are spread uniformly across the heatshield, from the top nose cone toward the inflatable ring (Fig. 3). To indicate the location of the sensor on the heatshield, a string of cubes is embedded on the surface along the longitudinal side of the cone. Specifically, five cubes in a series represent an FBG, in which each cube represents a grating (or sensor) in the core of the FBG. The locations of these red cubes serve as the sensing points where the deformation of the heatshield is measured.

IV. TESTING METHODOLOGY

A. HARDWARE SETUP

The aim is to link the described Blender simulation to a hardware mock-up of the heatshield and CubeSat [Fig. 4(a)]. A multicore fiber is slit into a polymer tube which is glued onto this mock-up [Fig. 4(b)]. This multicore fiber is a single fiber containing multiple cores dispersed in the cladding (Fig. 5). One channel is centrally located, while the other

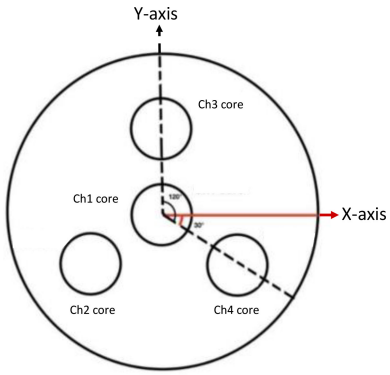

FIGURE 5. Spatial arrangement of the multicore fiber (cross section).

channels are off-center, making it easier to analyze the 3-D deformation forces. The red line in Fig. 5 shows the cross-sectional Cartesian coordinate system in the X-direction. This is used as a reference for the subsequent settings of the channels, X and Y axes in the model and in the data processing of the FBG. Take into account that the heatshield has an angle of 30° to the horizontal (Fig. 1). Hence, the X- and Y-deformation data of the FBG cannot be used directly in the Blender model. The X-axis deformations of the FBG need to be correctly mapped onto the x-, y-, and z-axes in the Blender model.

The different wavelengths used are 1529.98, 1539.01, 1547.68, 1557.01, and 1562.96 nm, having a window of 3 nm each. The FBGs are coupled to an FAZT I4E optical sensing instrument [32]. Due to the integration of four cores in a single fiber, a multiplexer is needed to combine and separate the signals of the four cores.

B. SOFTWARE SETUP

The deformations in the mock-up can be quantified in real-time using the simulation model. Therefore, Open Robot Control Software (OROCOS) is used [33]. The OROCOS framework is first used for the basic settings of the interrogator, such as the mean wavelength of each grating and the monitoring window intervals. Then, after obtaining the real-time wavelength data from the interrogator, the OROCOS program links to Robot Operating System (ROS). This allows real-time data readout connecting to external applications.

As the data read from the FBGs is accessed through an ROS node on a Linux system (programmed in C++), and the 3-D modeling of the heatshield is implemented through the Blender software (programmed in Python), it is necessary to find a solution for the data interaction between these two applications. The strategy to address this problem is to use a Socket communication mechanism based on the TCP/IP protocol [34].

C. REAL-TIME DATA READ-OUT SETUP

In order to perform a real-time data read-out process and simultaneously visualize the deformation in the Blender model, a specific roadmap is used [34]. The nature of

a socket is a mechanism for communication between different processes. It contains a series of different parameter files [34]. The main components include Relevant Protocols, Local Address, Local Port Number, Remote Address, and Remote Port Number.

After creating the ROS node and the subscription of TOPIC in Linux, the C++ code will create a socket with a specified IP address and a port number. The Python code in Blender will connect to this socket and listen to the contents of the socket according to the corresponding IP address and port number, thus enabling the real-time transfer of hardware data to the 3-D modeling application.

In Fig. 6, the heatshield monitoring process is shown.

In order to transform the sensor data into deformation data in the Blender model, a three-step approach is followed: 1) an initialization; 2) finding the magnitude of the force that creates a bend in the *x,y* direction taking the initialization phase into account; and 3) applying the force/deformation to the Blender model.

1) In the initialization process, the "stand-still" position, i.e., no bending, of the FBGs is used as the baseline. The wavelength values associated with this initial setup are measured, which are called the "offset values."
2) Additionally, the magnitude of the forces in *x*- and *y*-direction are obtained by comparing the measured wavelengths ("last data") with the ones measured in point 1 above ("offset").
   Using the formula below, the strain for each channel (ch) is obtained
   $$\text{Strain}_{ch} = k\ \frac{\text{last data}_{ch} - \text{offset}_{ch} - \text{offset}_{ch1}}{\text{offset}_{ch}} \quad (6)$$
   in which last data_{ch} is the wavelength measured in that specific channel (2, 3, or 4—see Fig. 5), offset_{ch} is the initial value of that specific channel (2, 3, or 4), and offset_{ch1} is the average value of the wavelengths of channel 1. k represents the constant relationship between the applied force and the deformation. The latter linear relationship is a simplification in the frame of this proof of concept and can be extended in future work.
   The cores are separated by 90°, 210°, and 330° (see also Fig. 5) related to the *x*-axis. Hence
   $$Fx_{ch\ n} = \text{Strain}_{ch\ n}\ .\ \cos\left(\text{angle}_{ch\ n}\right) \quad (7)$$
   $$Fy_{ch\ n} = \text{Strain}_{ch\ n}\ .\ \sin\left(\text{angle}_{ch\ n}\right) \quad (8)$$
   Taking into account the deformation obtained by all channels, the total force in *x*- and *y*-direction in the cross section is
   $$Fx_{\text{total}} = Fx_{ch\ 2} + Fx_{ch\ 3} + Fx_{ch\ 4} \quad (9)$$
   $$Fy_{\text{total}} = Fy_{ch\ 2} + Fy_{ch\ 3} + Fy_{ch\ 4}. \quad (10)$$
3) Since the multicore fiber is mounted at an angle of 30° to the horizontal (see Fig. 1), the *x*- and *y*-deformation data of the FBGs need to be converted taking into account an angle of 30° in the Blender model.

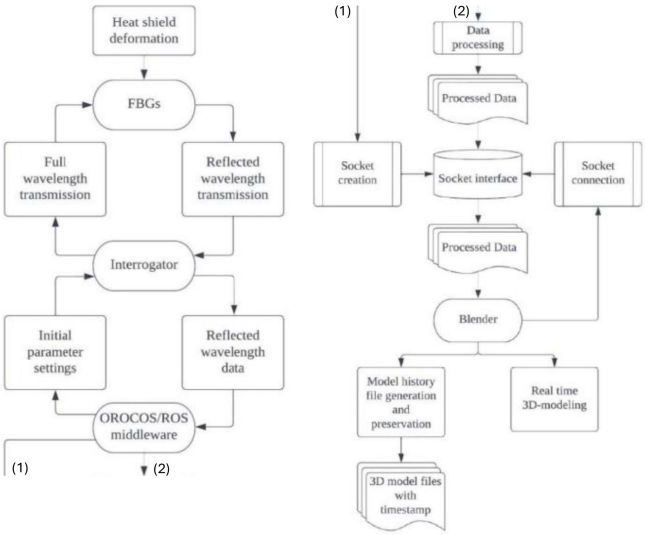

FIGURE 6. Heatshield monitoring process flowchart.

TABLE 1. Initial values of the coordinates of the sensing points.

Sensor	Initial mean wavelength [nm]	Window size [nm]	Coordinates (x,y,z)
1	1530.10	3	(1.67, 0.00, 2.35)
2	1539.17	3	(2.38, 0.00, 1.92)
3	1547.96	3	(3.13, 0.00, 1.48)
4	1557.11	3	(3.85, 0.00, 1.04)
5	1563.08	3	(4.55, 0.00, 0.62)

V. EXPERIMENTAL RESULTS

The four channel multicore fiber setup (Fig. 5) together with the flowchart (Fig. 6), enables the generation of the *X*, *Y*, and *Z* coordinates of the FBGs in different configurations. A calibration process was carried out in order to obtain valid deformation coordinates. The calibration process consists of different cases.

Case 1: The FBGs have no strain, hence the reflected wavelengths of the four channels (each having five sensors—an example is given in Table 1 for one channel) remain constant.

Case 2: Where a section of the FBGs has a uniform strain (the wavelengths of the four channels vary by the same amount), which means that it is in a state of axial tension or compression.

Case 3: Where the FBGs are subjected to bending but not an overall stretch. Hence, the FBGs are subjected to a strain that bends it but does not stretch or shrink them as a whole.

The actual bending may consist of cases 2 and 3. Since both cases are strain variations, the actual bend can be considered a linear superposition of cases 2 and 3. Since channel 1 is distributed on the central axis (see Fig. 5), the strain on channel 1 can be considered the average strain on the whole fiber. The ability of channels 2, 3, and 4 to measure the three spatial dimensions is due to their eccentric structure, which is arranged in a symmetrical configuration with an equal distance from the center and an angle of

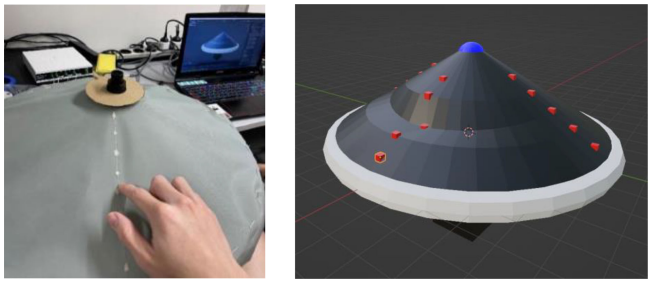

FIGURE 7. Physical and simulated heatshield downward deformation.

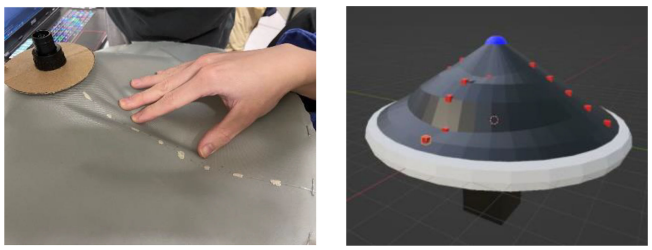

FIGURE 8. Physical and simulated heatshield multiple point deformation.

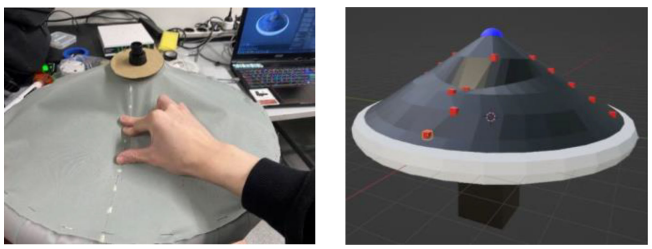

FIGURE 9. Physical and simulated heatshield complex deformation.

120° between the adjacent channels. The FBGs on these three channels will be more sensitive to the strain in both directions of their position in line with the axis.

The goal is to test the hardware setup in different circumstances: 1) pushing the heatshield downward; 2) pressing at multiple points simultaneously; and 3) a complex deformation. These tests show the real-time connection between the physical deformation of the heatshield and the visualization in the model.

A. DOWNWARD DEFORMATION TEST

Pressure is applied vertically downward on the surface of the heatshield at a location where the grating is installed and the sensing point on the surface of the corresponding 3-D model becomes recessed (Fig. 7).

As an example, the 4-channel data corresponding to the five gratings and the coordinates of the sensing points obtained by the algorithm are shown in Table 2.

B. MULTIPLE POINT DEFORMATION TEST

Pressing down vertically on the multiple mounting grating positions of the heatshield, the sensing points on the 3-D model surface are visible (Fig. 8).

TABLE 2. Wavelengths of the four channels and sensing points coordinates.

Sensor	Ch2 [nm]	Ch2 [nm]	Ch3 [nm]	Ch4 [nm]	Coordinates (x,y,z)
1	1530.03	1530.11	1530.06	1530.10	(1.69, 0.00, 2.40)
2	1539.05	1539.12	1539.10	1539.11	(2.39, 0.00, 1.94)
3	1547.88	1548.02	1547.88	1547.85	(2.95, 0.01, 1.18)
4	1557.02	1557.10	1557.05	1557.12	(3.83, 0.00, 1.01)
5	1563.00	1563.01	1563.15	1563.40	(4.52, 0.00, 0.58)

C. COMPLEX DEFORMATION TEST

Applying a composite force to the surface of the heatshield, the 3-D model shows the combined result of the vertical and longitudinal forces applied simultaneously (Fig. 9).

These results show that the physical deformation can be read-out in real-time and linked to the 3-D model. This information gives valuable insight in the deformation of the heatshield during reentry. Integrating these data into an onboard feedback system, would allow, using dedicated steering surfaces onto the heatshield, the creation of an adaptable reentry trajectory [6].

VI. CONCLUSION AND FUTURE WORK

In this research, FBGs are implemented inside a mock-up heatshield of a 3U reentry CubeSat in order to monitor the deformation of the heatshield. The results in Section V show that the physical deformation of the heatshield is measurable in real time using the 3-D simulation model. This conceptual design is a first step in having a full-size monitoring system based on FBGs which is implementable inside a CubeSat.

Future work consists of selecting applicable FBGs which fit the exact size and build-up of the heatshield. A more extended setup using multiple FBGs having more sensing points will allow a better full-size analysis of the heatshield. Also, using data interpolation between fiber cables could reflect the ability of the system to detect and pinpoint additional deformation sources.

The miniaturization of the interrogator is also part of future work, together with the analysis of how and if these integrated FBGs can be folded in order to fit inside the 1U. On the software side, the algorithms used in the current monitoring system can be further improved by optimizing the calculation processes. Using FBGs in these high-temperature environment comes with certain issues, such as crosstalk between strain and temperature. In order to avoid this, certain techniques can be applied, such as a strain-isolated FBG, or the use of specific coatings, such as gold or carbon.

The current acquisition rate used in the Blender software is 2.86 Hz. In order to reduce the response delay in real-life situations, further simulation tests should be done.

If the onboard generated data of the deformation during reentry is used in a feedback-loop, this allows the dedicated steering of the reentry trajectory by using specific flaps or additional inflatables on the heatshield. This steering process and additional hardware integration are also part of future work.

ACKNOWLEDGMENT

The authors would like to thank the Robotics Laboratory of the Department of Mechanical Engineering at KU Leuven for providing their lab facilities, the Faculty of Aerospace Engineering at TU Delft, the Advanced Integrated Sensing Lab of the Department of Electrical Engineering at KU Leuven, as well as the Aether team for making this research possible.

REFERENCES

[1] F. T. Bueno, "Towards the thousandth CubeSat: A statistical overview," *Int. J. Aerosp. Eng.*, vol. 2019, pp. 1–13, Jan. 2019.

[2] H. Tomio, "Commercially available imaging payloads for CubeSat earth observation missions," in *Proc. IEEE Aerosp. Conf. (AERO)*, Big Sky, MT, USA, Aug. 2022, pp. 1–19.

[3] R. Banerjee et al. "A 22-28 GHz polarization-reconfigurable flat-panel 8 × 8 Tx/Rx phased array antenna with uniquely arranged novel radiating elements for CubeSat communication," *IEEE Trans. Antennas Propag.*, vol. 71, no. 5, pp. 4138–52, May 2023.

[4] D. Sternberg, J. Essmiller, C. Colley, A. Klesh, and J. Krajewski, "Attitude control system for the mars cube one spacecraft," in *Proc. IEEE Aerosp. Conf.*, Big Sky, MT, USA, June. 2019, pp. 1–10.

[5] B. M. Walsh et al. "The cusp plasma imaging detector (CuPID) CubeSat observatory: Mission overview," *J. Geophys. Res. Space Phys.*, vol. 126, no. 4, pp. 1–17, Mar. 2021.

[6] J. Vanhamel, N. Eaton, and R. Spreij, "Using fiber Bragg gratings for shape monitoring and adjustment of a thermal protection system aboard a targeted re-entry CubeSat," in *Proc. 2nd Int. Conf. Flight Veh., Aerothermo-Dyn. Re-Entry Missions Eng. (FAR)*, Heilbronn, Germany, Jun. 2022, pp. 19–23.

[7] S. J. Mihailov, "Fiber Bragg grating sensors for harsh environments," *Sensors*, vol. 12, no. 2, pp. 1898–1918, Feb. 2012.

[8] K. S. Lay, L. Li, and M. Okutsu, "High altitude balloon testing of Arduino and environmental sensors for CubeSat prototype," *HardwareX*, vol. 12, Jun. 2022, Art. no. e00329.

[9] P. Visser and J. A. A. Van den Ijssel, "Orbit determination and estimation of non-gravitational accelerations for the GOCE reentry phase," *Adv. Space Res.*, vol. 58, no. 9, pp. 1840–1853, Nov. 2016.

[10] G. Hegde, S. Asokan, and G. Hedge, "Fiber Bragg grating sensors for aerospace applications: A review," *ISSS J. Micro Smart Syst.*, vol. 11, no. 1, pp. 257–275, Apr. 2022.

[11] S. Gilbertson et al., "High speed, localized multi-point strain measurements on a containment vessel at 1.7 MHz using swept-wavelength laser-interrogated fiber Bragg gratings," *Sensors*, vol. 20, no. 20, pp. 1–28, 2020.

[12] P. F. S. Rosa et al., "An FBG optical approach to thermal expansion measurements under hydrostatic pressure," *Sensors*, vol. 17, no. 11, p. 2543, Nov. 2017.

[13] S.-Z. Chen, D.-C. Feng, and W.-S. Han, "Comparative study of damage detection methods based on long-gauge FBG for highway bridges," *Sensors*, vol. 20, no. 13, p. 3623, 2020.

[14] Y. Du, B. Sun, J. Li, and W. Zhang, *Optical Fiber Sensing and Structural Health Monitoring Technology*, 1st ed. Singapore: Springer, 2019.

[15] P. M. Toet, R. A. J. Hagen, H. C. Hakkesteegt, J. Lugtenburg, and M. P. Maniscalco, "Miniature and low cost fiber Bragg grating interrogator for structural monitoring in nano-satellites," in *Proc. Int. Conf. Space Opt. (ICSO)*, Canary Islands, Spain, 2017, Art. no. 105631E.

[16] A. D. Kersey et al., "Fiber grating sensors," *J. Lightw. Technol.*, vol. 15, no. 8, pp. 1442–1463, Aug. 1997.

[17] A. Gizatulin, L. Meshkov, I. Vinogradova, V. Bagmanov, E. Grakhova, and A. Sultanov, "Generation of vortex optical beams based on chiral fiber-optic periodic structures," *Sensors*, vol. 20, no. 18, pp. 1–16, 2020.

[18] (TNO, The Hague, The Netherlands). *Piezoelectric Assisted Smart Satellite Structure*. Sep. 2018. [Online]. Available: https://cordis.europa.eu/project/id/312216/reporting

[19] (Consiglio Nazionale Delle Ricerche, Rome, Italy). *Fiber Optic Sensors Application for Structural Health Monitoring*. Mar. 2015. [Online]. Available: https://cordis.europa.eu/project/id/255865

[20] I. McKenzie et al., "Fiber optic sensing in spacecraft engineering: An historical perspective from the European space agency," *Front. Phys.*, vol. 9, Nov. 2021, Art. no. 719441.

[21] A. Othonos, K. Kyriacos, and E. K. Glenn, "Fiber Bragg gratings: Fundamentals and applications in telecommunications and sensing," *Phys. Today*, vol. 53, no. 5, pp. 61–62, May 2000.

[22] J. Wei, Y. Hao, Y. Fu, L. Yang, J. Gan, and H. Li, "Experimental study on glaze icing detection of 110 kV composite insulators using fiber Bragg gratings," *Sensors*, vol. 20, no. 7, p. 1834, 2020.

[23] I. Gouzman et al., "Advances in polyimide-based materials for space applications," *Adv. Mater.*, vol. 31, no. 18, Feb. 2019, Art. no. 1807738.

[24] T. Erdogan, "Fiber grating spectra," *J. Lightw. Technol.*, vol. 15, no. 8, pp. 1277–1294, Aug. 1997.

[25] G. Guo, "Superstructure fiber Bragg gratings for simultaneous temperature and strain measurement," *Optik*, vol. 182, pp. 331–340, Apr. 2019.

[26] H. Alemohammad, "Superstructure fiber Bragg grating sensors for multiparameter sensing," in *Opto-Mech. Fiber Opt. Sens.*, 1st ed., H. Alemohammad Ed., Amsterdam, The Netherlands: Elsevier Inc., 2018, pp. 27–47.

[27] L. Zixuan, Y. Fengming, S. Osamu, and O. Yoji, "In-situ laser-ultrasonic visualization with the use of regenerated fiber Bragg Grating sensors at elevated temperatures," *Mech. Syst. Signal Process.*, vol. 188, Apr. 2023, Art. no. 110007.

[28] *Fiber Optic Essentials*, 1st ed., C. DeCusatis, Ed., Waltham, MA, USA: Acad. Press, 2006.

[29] L. Cheng and B. Ahlers, "Vega interstage strain measurements: Comparison between conventional strain gauges and fibre Bragg grating sensors," in *Proc. SPIE 6th Int. Conf. Space Optics (ICSO)*, Noordwijk, The Netherlands, 2017, Art. no. 105672E.

[30] F. Aihen, C. Daolun, L. Cheng, and G. Xijia, "Flat-cladding fiber Bragg grating sensors for large strain amplitude fatigue tests," *Sensors*, vol. 10, no. 8, pp. 7674–7680, Aug. 2010.

[31] "The Blender foundation." Blender. Oct. 2019. [Online]. Available: https://www.blender.org/download/

[32] "FAZT I4G-16 interrogator," Dataset, Femto Sens. Int., Atlanta, GA, USA, 2018. [Online]. Available: https://femtosensing.com/wp-content/uploads/2018/09/FAZ-I4-16-Interrogator-Datasheet-V3.pdf

[33] H. Bruyninckx, "Open robot control software: The OROCOS project," in *Proc. ICRA. IEEE Int. Conf. Robot. Autom.*, Seoul, South Korea, 2001, pp. 2523–2528.

[34] H. Si, C. Sun, B. Chen, L. Shi, and H. Qiao, "Analysis of socket communication technology based on machine learning algorithms under TCP/IP protocol in network virtual laboratory system," *IEEE Access*, vol. 7, pp. 80453–80464, 2019.

JURGEN VANHAMEL (Senior Member, IEEE) was born in Hasselt, Belgium, in 1978. He received the bachelor's degree in mathematics from KHLim, Hasselt, in 1999, the M.Sc. degree in industrial sciences, electronics, option information, and communication technology from PXL-XIOS, Diepenbeek, Belgium, in 2003, the postgraduate degree in avionics and spacionics from KHBO, Ostend, Belgium, in 2011, and the Ph.D. degree from the Faculty of Engineering Technology, KU Leuven, Leuven, Belgium, in 2020.

He was a Project Engineer with the Royal Belgian Institute for Space Aeronomy, Brussels, Belgium, where he was involved in multiple ESA space mission (PICASSO, ALTIUS, and EnVision) and also several other ground-based projects. He is currently an Assistant Professor with the Faculty of Aerospace Engineering, TU Delft, Delft, The Netherlands, and a Visiting Professor with the Advanced Integrated Sensing Lab, Department of Electrical Engineering, KU Leuven. His research focusses on the RF driving system for acousto-optical devices, as well as fiber Bragg gratings. Additionally, he is interested in space weather (i.e., ionospheric analysis) using dedicated RF systems and antenna setups.

Dr. Vanhamel is a member of the Belgian Engineering Society IE-Net, the National Radio-Amateur League UBA, Belgium, the Royal Belgian Air Force Radio Association (BAFARA), and the European Aeronautics Science Network.

KIN CHIO CHAO was born in Macau, SAR, China, on 1 February 1998. He received the B.Eng. degree in automation from Tianjin University, Tianjin, China, in 2022, and the B.Sc. degree in engineering technology and the M.Sc. degree in electronics and ICT engineering technology from the Catholic University of Leuven, Leuven, Belgium, in 2022 and 2023, respectively.

His research interests lie in the area of embedded systems, focusing on data acquisition and real-time systems for efficient monitoring and control applications.

YIFENG CHEN was born in Ningxia, China, in March 2000. He received the bachelor's degree in automation from Tianjin University, Tianjin, China, in 2022, and the bachelor's degree (with Hons.: cum laude) in electronics engineering and the master's degree (with Hons.: cum laude) in electronics and ICT engineering technology from KU Leuven, Leuven, Belgium, in 2022 and 2023, respectively.

During his master's studies, he focused on the development of a real-time monitoring system for satellite thermal protection using fiber Bragg grating sensors. He is currently a Hardware Systems Engineer with Apple Inc., Cupertino, CA, USA, where he is responsible for the hardware design and development of next-generation iPad products. He has contributed to the successful launch of the 2024 iPad Pro and iPad Mini. His research involved both physical modeling and software simulations, demonstrating the feasibility and effectiveness of fiber Bragg grating sensors in this application.